Effect of exfoliation and surface deposition of MnOx species in g-C3N4: Toluene photo-degradation under UV and visible light

Mario J. Muñoz-Batista *, Olga Fontelles-Carceller, Anna Kubacka *, Marcos Fernández-García

Instituto de Catálisis y Petroleoquímica, CSIC, C/Marie Curie 2, 28049 Madrid, Spain

ABSTRACT

A relatively low surface area graphitic carbon nitride produced by a standard melamine calcination procedure was subjected to an exfoliation process and/or surface deposition of Mn-containing species. The resulting catalysts were characterized using X-ray diffraction and photoelectron spectroscopies, transmission electron microscopy, UV–vis and infrared spectroscopies, and porosimetry. The photocatalytic properties of the materials were tested in the gas-phase degradation of toluene under UV, visible and Sunlight-type illumination and their performance assessed through the measurement of the materials optical properties and subsequent calculation of the true quantum efficiency. The numerical analysis of the efficiency parameter evolution throughout the above mentioned carbon nitride samples provides quantitative estimation of the catalytic effect resulting from the exfoliation process and/or the surface deposition of Mn-containing species. Such analysis allows thus to compare the activity significance of each one of the carbon nitride modifications explored as well as the synergistic effect originated by the combined action of such modifications.

© 2016 Elsevier B.V. All rights reserved.

1. Introduction

The high levels of pollution originated by industrial and mobile source emissions, together with the ever-higher standards for emission control of many industrialized countries, have driven the current interest in environmental protection processes, leading to a high scientific and technological activity in this area. In this context, much attention has been focused on advanced oxidation processes and in particular heterogeneous photocatalysis. Heterogeneous photocatalysis is an advanced oxidation process that uses semiconductors, broadly applied in the degradation/transformation of organic pollutants as well as biological microorganisms [1–4]. Its most significant advantage with respect to other remediation technologies could be the use of the solar energy, a free and renewable energy source. Obviously, the efficiency of this process depends directly of the photocatalyst performance upon solar irradiation conditions.

Undoubtedly, TiO_2 has been the most studied photocatalyst. For such material, many studies reported relatively high activity. Addi-

tionally, its low cost and stability makes this material particularly interesting for a wide variety of applications [1,5–8]. However, the limited utilization of the visible and infrared regions of the solar spectrum precludes its wide potential application as a solar photocatalyst. Such limitation comes from the high band gap inherent by all titania polymorphs, around 3.0–3.5 eV [1,7,9–13]. Thus, and despite the significant use of TiO_2-based heterogeneous photocatalysts, it is especially important the development of new, alternative semiconductors focusing in the effective utilization of the sunlight. This involves unavoidably the improvement of the visible light use as this region accounts for ca. 43% of the intensity of the solar spectrum.

One of the materials potentially interesting for sunlight-driven photocatalytic applications is the graphite like carbon nitride (g-C_3N_4). Its good electronic and chemical properties and thermal stability have allowed the use of the g-C_3N_4 material as a free metal catalysis for many photochemical reactions such as organic photodegradation, water splitting or alcohol reforming [14–19]. In order to optimize the carbon nitride catalytic properties for target-specific applications, several modifications of bare g-C_3N_4 have been conducted, including the surface modification using metals such as Ag, Au, Pt [20–30], and different oxides or hydroxides, among which we can highlight ZnO_2, TiO_2, WO_3, Cu_2O, $Co(OH)_2$ and MnO_xOH_y [31–41]. Another possible modification consists

in obtaining exfoliated systems. This greatly increases the surface area of the g-C_3N_4 bulk. The limited surface area presented by the bulk material, typically 10–40 m^2g^{-1}, is a consequence of the stacking of the g-C_3N_4 layers and can be significantly increased by the mentioned exfoliation process [15,20,30,42,43]. Moreover, many authors report that exfoliated g-C_3N_4 nanomaterials can modify positively the photo-charge handling capability of the material with respect to the bulk counterpart [16,44–46]. There are several methods of exfoliating g-C_3N_4. One of the simplest is the ultra-sonication assisted by water. In this case, the exfoliated g-C_3N_4 material presents high stability and lacks toxic impurities (common by other preparation methods), which make them a promising material for photocatalytic processes [44].

In this contribution we combine two strategies related to the exfoliation and surface modification by Mn-containing species to obtain a new material which enhanced catalytic properties with respect to the bare, bulk-type g-C_3N_4. Mn-containing species have attracted particular attention due to their significant influence in photoactivity through the efficient handling of hole-related species while exfoliation appears, as mentioned, as a general way to improve photo-performance [39]. We tested such materials in the photodegradation of gas phase toluene. In order to fully analyze the potential of the materials in utilizing efficiently the sun as the energy source of the photodegradation process, the study was carried out using three light sources, this is; UV, sunlight-type and visible type. The characterization of the samples was performed using X-ray diffraction, X-ray photoelectron, infrared, and ultraviolet spectroscopy, transmission electron microscopy and N_2 physisorption. Additionally, the study includes the modelling of the light-matter interaction, necessary for determining the true quantum efficiency values and compare samples in quantitative basis. Using the true quantum efficiency parameter and a simple mathematical procedure we carried out a quantitative analysis of the beneficial effects induced by the exfoliation process of the carbon nitride and/or the presence of Mn-containing species in the photoactivity of the materials.

2. Materials and methods

2.1. Samples preparation

The graphitic carbon nitride was obtained by calcination of melamine (Aldrich), in a semi-closed system to prevent sublimation, at 580 °C for 4 h using a heating ramp of 5 °C min^{-1} [20,39,47]. The exfoliated g-C_3N_4 material was prepared by ultrasonication for 4 h using as-prepared bulk g-C_3N_4 in deionized water (1 mg cm^{-3}). The suspended part after 18 h of sedimentation was selected as the exfoliated part of the material and obtained after evaporation of the water at 80 °C. The carbon nitride component modified with manganese oxide was prepared using an impregnation method. For this, the g-C_3N_4 or the exfoliated one and the manganese precursor (Manganese (II) nitrate tetrahydrate, Aldrich) were added to a deionized water solution. After 2 h under magnetic stirring the liquid was evaporated at 110 °C for 15 h. The final MnO_x-carbon nitride composites were obtained by calcination at 350 °C, with a heating ramp of 5 °C min^{-1} maintaining this temperature for 2 h. The final MnO_x loading was 2 wt.%, confirmed with an error below 5% using ICP-AAS (induced couple plasma and atomic absorption spectroscopy) spectrometry.

Samples names are g-C_3N_4 or g-C_3N_4/MnO_x when prepared from the initial powder extracted from calcination of melamine and E-g-C_3N_4 or E-g-C_3N_4/MnO_x when prepared from the powders subjected to the exfoliation procedure.

2.2. Characterization and analytical methods

The BET surface areas and average pore volumes and sizes were measured by nitrogen physisorption (Micromeritics ASAP 2010). XRD profiles were obtained using a Seifert D-500 diffractometer using Ni-filtered Cu Kα radiation with a 0.02° step. UV–vis diffuse-reflectance spectroscopy experiments were performed on a Shimadzu UV2100 apparatus using nylon as a reference. The Fourier transform infrared spectra were taken in a Bruker Vertex 80 FTIR spectrometer sing a MCT detector. XPS data were recorded on 4×4 mm2 pellets, 0.5 mm thick, prepared by slightly pressing the powered materials which were outgassed in the prechamber of the instrument at room temperature up to a pressure $<2 \times 10^{-8}$ Torr remove chemisorbed water from their surfaces. The SPECS spectrometer main chamber, working at a pressure $<10^{-9}$ Torr, was equipped with a PHOIBOS 150 multichannel hemispherical electron analyser with a dual X-ray source working with Ag Kα (hν = 1486.2 eV) at 120 W, 20 mA using C 1s as energy reference (284.6 eV). Transmission electron microscopy images were recorded on a JEOL 2100F TEM/STEM microscope.

2.3. Photo-catalytic experimental details

Gas-phase photo-oxidation of toluene ($\geq$99% Aldrich) was carried in a continuous flow annular photoreactor containing ca. 0.4 mg cm^{-2} of photocatalyst as a thin layer coating on a pyrex tube. The scheme of the reaction system is presented in Fig. 1 and has been presented and detailed in previous works [48,49]. The reacting mixture (100 ml min^{-1}) was prepared by injecting toluene into a wet (ca. 75% relative humidity) 20 vol.% O_2/N_2 flow before entering to the photoreactor, yielding an organic inlet concentration of ca. 700 ppmv. Fluorescent UV (Sylvania F6WBLT-65; 6 W) and sunlight-type lamps (Sylvania F6W/D; 6 W) were used for the photoreaction experiment. For the visible light experiments, we used a flexible polyester filter made from a deeply dyed PET material to absorb ultraviolet rays. The material allows less than 10% transmission below 390 nm. Reaction rates and selectivity were evaluated under steady-state conditions, typically achieved after ca. 6–10 h from the irradiation starting. The concentration of toluene and the reaction products were analyzed using an on-line gas chromatograph (Agilent GC 6890) equipped with a TCD (for CO_2 measurement) and FID (organics measurement) detectors.

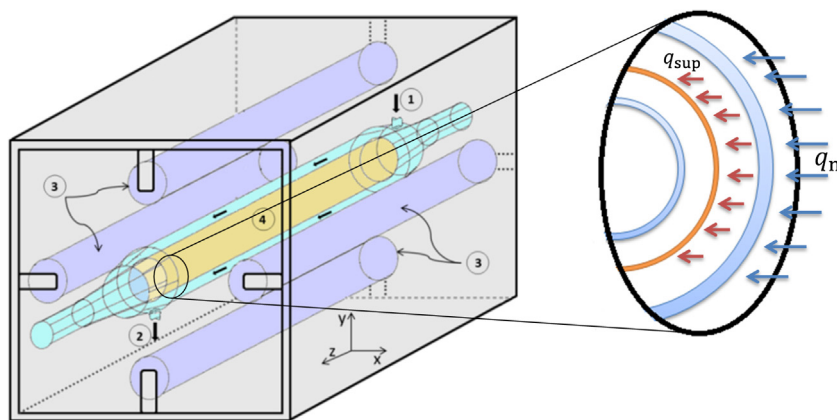### 2.4. Light-matter interaction modelling and quantum efficiency calculation

2.4.1. Local superficial rate of photon absorption

The local superficial rate of photon absorption ($e^{a,s}$) is defined by Eq. (1) [31,50]. In this equation F_{As} is the fraction of light absorbed by the sample and q_{sup} the radiation flux at each position (Xs,Ys,Z_s) of the catalytic film (See Fig. 1).

$$e^{a,s}(\underline{x}) = q_{sup}(\underline{x}) F_{As} \tag{1}$$

To obtain the radiation flux on the surface of the samples, we calculate first the impinging radiation flux from the lamps (q_n in Fig. 1). Considering the coordinated system presented in Fig. 2 and the geometry of the reactor (annular multilamp), the q_n can be determined by Eq. (2) [31].

$$q_n(Xs, Ys, Z_s) = \sum_{L=1}^{L=4} \sum_{\lambda} \int_{\varphi_{min,L(x,y)}}^{\varphi_{max,L(x,y)}} \int_{\theta_{min(x,y,\varphi)}}^{\theta_{max(x,y,\varphi)}} \frac{P_{\lambda,L}}{2\pi R_L Z_L} \sin^2\theta$$

$$\left((\frac{X_s - X_L}{R})\cos\varphi + (\frac{y_s}{R})\sin\varphi \right) d\varphi d\theta \tag{2}$$

Fig. 1. Photocatalytic annular reactor scheme. (1) gas inlet, (2) gas outlet, (3) lamps, (4) catalyst sample. q_{sup} radiation flux on the surface of the sample (red), q_n radiation flux from the lamps (blue). (For interpretation of the references to colour in this figure legend, the reader is referred to the web version of this article.)
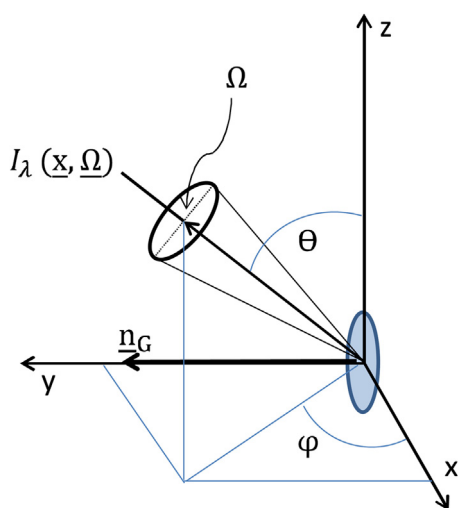
Fig. 2. Coordinated system. Center of coordinates located at the sample (defined by coordinates x_s, y_s, z_s).

Where the integration limits can be evaluated using the ray tracing method and are summarized in Eqs. (3)–(10) [31,51].

$$\varphi_1 = \tan^{-1}\left(\frac{X_L - X_s}{Y_L - Y_s}\right) \tag{3}$$

$$\varphi_2 = \sin^{-1}\left(\frac{R_L}{(X_L - X_s)^2 + (Y_L - Y_s)^2}\right) \tag{4}$$

$$\varphi_{min} = \varphi_1 - \varphi_2 \tag{5}$$

$$\varphi_{max} = \varphi_1 + \varphi_2 \tag{6}$$

$$\theta_{min}(\varphi) = \cos^{-1}\frac{-Z_s}{(X_{Lm}(\varphi) - X_s)^2 + (Y_{Lm}(\varphi) - Y_s)^2 + Z_s^2} \tag{7}$$

$$\theta_{max}(\varphi) = \cos^{-1}\frac{Z_L - Z_s}{(X_{Lm}(\varphi) - X_s)^2 + (Y_{Lm}(\varphi) - Y_s)^2 + Z_s^2} \tag{8}$$

Where:

$$X_{Lm}(\varphi) = X_L + (X_s - Y_L)\cos\varphi^2 + (Y_L - Y_s)(\cos\varphi\sin\varphi) - \sin\varphi\sqrt{(R_L^2 - (X_s - X_L)\cos\varphi + (Y_L - Y_s)(\sin\varphi)^2)} \tag{9}$$

$$Y_{Lm}(\varphi) = Ys_i + (Y_L - Y_s)\cos\varphi^2 + (X_s - X_L)(\cos\varphi\sin\varphi) - \cos\varphi\sqrt{(R_L^2 - (X_s - X_L)\cos\varphi + (Y_L - Y_s)(\sin\varphi)^2)} \tag{10}$$

X_L, Y_L, Z_L are the coordinates of the points located on the surface of the lamp. Xs, Ys and Zs are the coordinates of the points located on the surface of the films.

Finally, the q_{sup} x/y components (see Figs. 1 and 2; Eq. (11)) can be determined using q_n and a radiation balance, which considers the main optical (Transmittance/Absorbance and Reflectance) events occurring in all components of the reactor placed between the emission source and catalyst, i.e. glass and reaction media, as well on the catalytic film.

$$q_{sup} = \sqrt{{}^xq^2 + {}^yq^2} \tag{11}$$

A detailed description of the mathematical formulation to provide q_{sup} as a function of q_n (Eq. (2)) and the transmittance/reflectance optical measurements for each component of our reactor system can be found elsewhere [31] and is summarized at the Supporting information section.

2.4.2. Quantum efficiency

Quantum efficiency values (η_q) were determined using Eq. (12) [7,52–57]. This work presents the determination of the true quantum efficiency using a stringent approach for calculating the light-matter interaction in the reactor (described previously in sub-section 2.4.1) and including explicitly the selectivity towards the reaction products as a way to measure the number of charge species involved in the generation of each reaction product (see Eq. (12)).

$$\eta_q = \frac{r}{e^{a,s} \times S} \times 100 \tag{12}$$

Where r is the reaction rate (mol m^{-2} s^{-1}), $e^{a,s}$ the superficial rate of photon absorption (Einstein m^{-2} s^{-1}; Eq. (1)) and S is the aforementioned Selectivity factor (dimensionless). This last factor can be determined using Eq. (13) [31].

$$S = \sum_i n_i\, S_i \tag{13}$$

Were i runs over all products of the reaction, S_i and n_i are the fractional selectivity to product i, and the inverse of the number of charge carrier species required to obtain the specific i product.

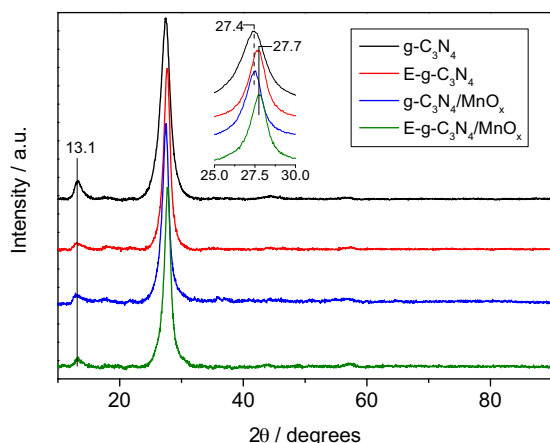The Supporting information section summarizes the procedure to calculate the n_i factors.

Fig. 3. XRD spectra for the carbon nitride based samples.

Fig. 4. UV−vis spectra for the carbon nitride based samples.

3. Results and discussion

3.1. Characterization results

Morphological properties determined by N_2 physisorption are summarized for all materials studied in Table 1. First of all, the specific superficial area values show differences between the bulk and exfoliated g-C_3N_4 species. An increase in the BET surface area for the delaminated g-C_3N_4 is detected, being larger than 290% with respect to the bulk system in all cases (i.e. in presence or absence of manganese surface species). This enhancement factor of the surface area is in line with those reported in the literature [14–19]. In addition, a modest decrease in the surface area parameter is detected when the Mn component is included in both carbon nitride samples. Table 1 also shows pore volume and pore size values of the photocatalysts. The values of these observables present a similar behavior to those of the BET surface area, this is, in all cases we observe a somewhat modified, lower porosity for samples containing MnO_x species. These results suggest that MnO_x particles tend to be located in the porous structure of the g-C_3N_4, occluding it partially.

The X-ray diffraction patterns for the bulk and exfoliated carbon nitride samples are shown in Fig. 3. All samples display the typical spectra of the graphitic g-C_3N_4 layered structure, dominated by the interlayer-stacking (002) reflection. The (100) reflection, related to the interlayer structural packing motif of tri-s-triazine units, is also detected clearly in all samples at around 13.1° [20]. It is important to note that using this technique; it has not been possible to obtain information about the MnO_x minority phase. Finally, a 0.3° shift is detected in the (002) reflection for the exfoliated vs. the bulk samples, as a token related to the interlayer distance decrease taking place during the exfoliation process. It has been hypothesized that the limitation of the number of sheets stacked produces the weakening of interlayer forces with effect in the corrugation of the layer(s) and the subsequent decrease of the corresponding distance between layers [45].

Optical properties are, obviously, especially important for photocatalytic applications. Here we examined such properties using UV–visible spectroscopy. In Fig. 4, we present the spectra of the samples; they display a profile dominated by the g-C_3N_4 component, leading to band gap values reported in the last column of Table 1. These values are calculated considering the materials indirect band gap semiconductors [15]. The Fig. 4 zoom view highlights the typical blue shift observed for exfoliated g-C_3N_4 samples [45], which entails a band gap increment of ca. 0.1 eV (Table 1). This variation can be ascribed to the quantum confinement effect derived
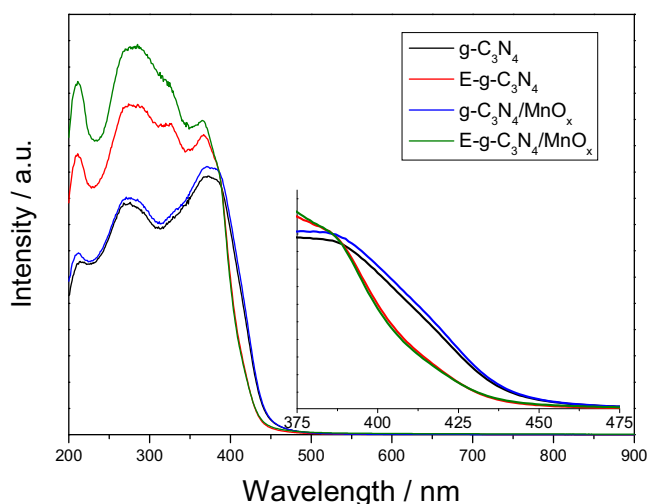

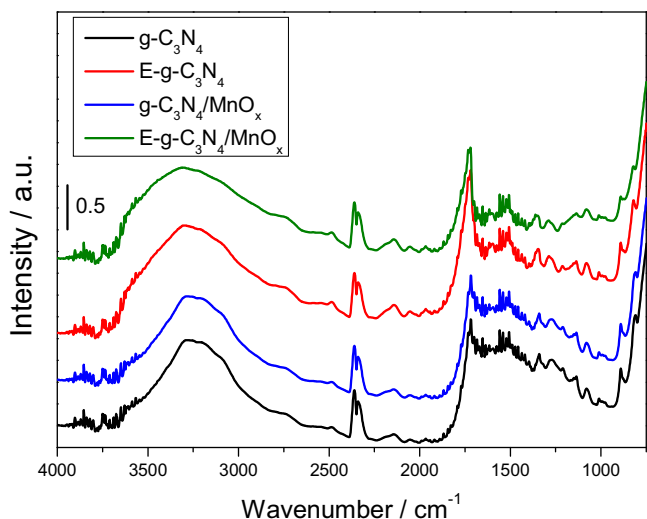**Fig. 5.** FTIR spectra for the carbon nitride based samples.

from the limitation on the stacking of CN-containing layers in the g-C_3N_4 nanosheet-like structure [58].

Infrared spectra of the samples obtained at RT condition are shown in Fig. 5. The N−H stretching vibration contributions at the 3500–2500 cm^{-1} region are present in all samples [43,58]. In this region we have an additional contribution coming from adsorbed water molecules. The shape of this broadband shows small differences between the bulk and exfoliated samples. In the case of the exfoliated one, the band seems to be wider which could be related with an increase of the water adsorption on the surface. In the 1600–1200 cm^{-1} regions we can observe several contributions mostly associated to stretching modes of CN heterocyclic moieties [59–62]. Specific differences between bulk and exfoliated samples are mostly detected around 1700 cm^{-1} and may reinforce the idea that exfoliated materials have a more water-prone, hydrophilic surface. Structural differences in the C−N network can be additionally invoked to justify the differences observes between the exfoliated and bulk materials. Finally, around 850–800 cm^{-1} we note additional contributions coming from the breathing modes of tris-s-triazine, which confirms that all samples maintain the g-C_3N_4 block structure within the CN-containing layers, in spite of the differences in the dimension of their layer stacking [43,45,58,63].

Table 1
Morphological and Optical properties for the carbon nitride based samples.[a]

Sample	BET Surface area ($m^2 g^{-1}$)	Pore volume ($cm^3 g^{-1}$)	Pore size (nm)	Band Gap (eV)
g-C_3N_4	21.8	0.103	15.1	2.7
E-g-C_3N_4	63.4	0.210	15.7	2.8
g-C_3N_4/MnO_x	17.9	0.074	15.7	2.7
E-g-C_3N_4/MnO_x	52.3	0.170	16.2	2.8

[a] Standard error: BET, $1.5 m^2 g^{-1}$; porosity, 8%.
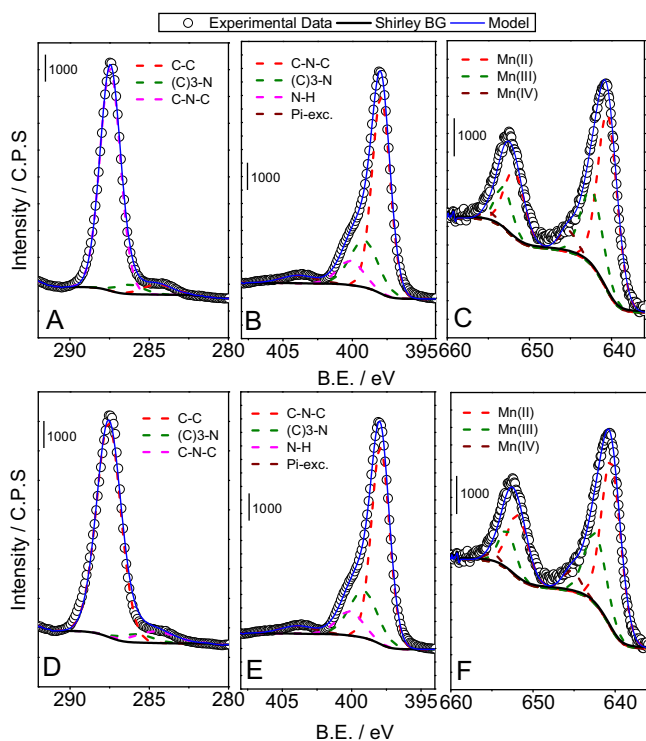
Fig. 6. Cs (A), N1s (B) and Mn 2p (C) XPS spectra for the g-C_3N_4/MnO_x sample. C1s (D), N1s (E) and Mn 2p (F) XPS spectra for the E-g-C_3N_4/MnO_x sample. Fitting results display the different contributions to each XPS peak.

The structural analysis of the materials is completed with the help of the X-ray photoelectron spectroscopy. Fig. 6 displays XPS data for the two samples containing manganese and concerning the carbon 1s (C1s) nitrogen 1s (N1s), and manganese 2p (Mn2p) experimental regions and fitting results. No significant differences were observed between the corresponding bulk or exfoliated samples in presence or absence of MnOx species. A full summary of the fitting outcome is presented at the Supporting information section Tables S2 (for C1s) and S3 (for N1s). In Table S3 we also included information concerning the C/N atomic ratio. For C1s we detected the C—C (which has a contribution for spurious entities besides that of the main component of the sample) signal as well as those contributions related bridging carbons between aromatic moieties (C$_3$—N) or at the aromatic rings (N—C—N). For N1s the fitting takes into account the last two species mentioned as well as the contribution from N—H moieties [15,64–66]. The fitting results summarized in Tables S2 and S3 provide evidence of the strong similitude detected between all samples. A mild difference is measured in the C/N ratio, with an increase for exfoliated vs. bulk samples, as previously detected by other authors as the stacking of carbon nitride layers diminished [64,65].

The XPS study also renders information about the MnO$_x$ component. The fitting indicate the presence of a mixture of Mn(II), Mn(III) and Mn(IV) states in both bulk and exfoliated carbon nitride samples where the Mn component is present (see results at Table

S4) [67]. This mixture has been already detected in similar samples [39]. Here we observed rather small contributions of the most oxidized Mn (IV) species while the other two chemical states dominate the spectra. Most important, absence of significant differences is noted between the Mn chemical state when supported on bulk or the exfoliated materials. The differences in the carbon nitride component do not affect the Mn oxidation state. This is a consequence of the similar interaction as well as Mn dispersion. In fact, the Mn/(C+N) atomic ratio determined by XPS show limited differences (0.014 for g-C_3N_4 and 0.012 for E-g-C_3N_4).

To end up the physico-chemical characterization of the catalysts, morphological differences between the exfoliated and bulk components are further investigated through a TEM study (Fig. 7). The A and B micrographs correspond to the g-C_3N_4 and g-C_3N_4/MnO_x samples, respectively. Both display several darker areas caused by the stacking of a significant number of carbon nitride sheets. On the other hand, the E-g-C_3N_4 and E-g-C_3N_4/MnO_x catalysts (C and D) show a nanosheet-type structure, with significant less interference or shadowing effects coming from the stacking of carbon nitride layers. The differences in the stacking of layers between the bulk and the exfoliated specimens are also evident in the low magnification SEM images presented at the Supporting information section (Fig. S4). The presence of the Mn is not inferred from the microscopy study.

In summary all structural (XRD, microscopy, infrared) and electronic (UV–vis, XPS) studies showed up physico-chemical differences, all of them (but particularly XRD, TEM and UV–vis) consistent with the limitation of the stacking dimension of CN-containing layers in the materials. Of prime importance is that they produced differences in band gap energy and thus can have significance in light absorption and charge handling properties and thus in photocatalytic properties. Concerning the manganese species, XPS results did not detect differences between the chemical state of this component in the bulk and exfoliated samples. A rather mild variation in the dispersion of Mn is however encountered, with a modest increase in the case of the exfoliated vs. the bulk material.

3.2. Photocatalytic elimination of toluene

The photochemical performance of the obtained materials in elimination of toluene under UV, visible, and sunlight-type illumination is reported in Fig. 8. The reaction rate is maximized under UV excitation but relatively close (although inferior considering the error of the measurement) values are obtained upon sunlight-type excitation. Significantly lower values are encountered while using exclusively visible light excitation. The exfoliated samples are clearly superior to the bulk ones and the presence of MnO$_x$ seems to affect activity as a function of the nature (bulk or exfoliated) of the carbon nitride main component. Compared with the P25 reference sample indicates relatively low rates under UV and Sunlight-type but, on the contrary, the carbon nitride samples display a significant increase on the reaction rate under visible light illumination due to the almost null performance of P25 in such conditions [68–70]. Note that P25/Titania catalysts works through a hydroxyl or hole-related mechanism [33]. while the carbon nitride samples are only able to produce (at least initially) electron-related charged species [20,71],
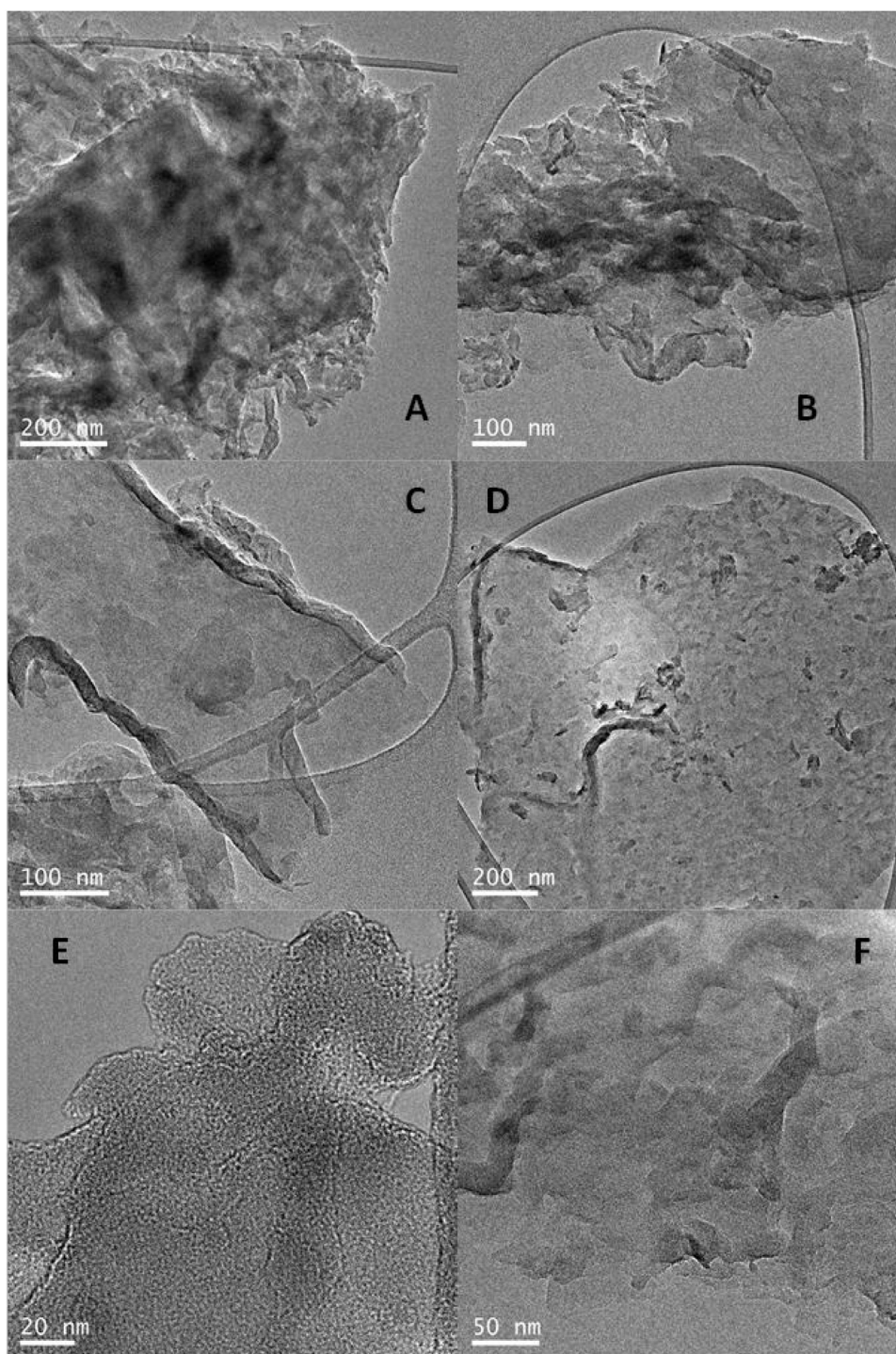
Fig. 7. TEM views of (A) bulk g-C_3N_4, (B) bulk g-C_3N_4 modified with MnO_x, (C) and (E) g-C_3N_4 exfoliated, and (D) and (F) g-C_3N_4 exfoliated modified with MnO_x.

indicating that the comparison of both types of samples is complex. In any case, comparison with Ag-promoted carbon nitride materials shows a less significant effect of MnO_x for a bulk carbon nitride material having a similar loading that here tested [72]. MnO_x surface species have however a different behavior in the exfoliated material. Samples differ in activity (Fig. 8), as already discussed in this paragraph, but also in selectivity (Table 2). Selectivity differences are mostly encountered in presence/absence of MnO_x species as well as with the nature of the illumination source. The latter is relatively modest and any case minor with respect to the first.

Table 2

Reaction selectivity of toluene photodegradation.[a]

Sample	UV		Sunlight-type		Visible	
	Bz[b]	CO_2	Bz[b]	CO_2	Bz[b]	CO_2
g-C_3N_4	46	54	41	59	58	42
E-g-C_3N_4	42	58	44	56	49	51
g-C_3N_4/MnO_x	56	44	58	42	60	40
E-g-C_3N_4/MnO_x	51	49	61	39	63	37

[a] Average Standard error: 4.3%.

[b] Bz: benzaldehyde.

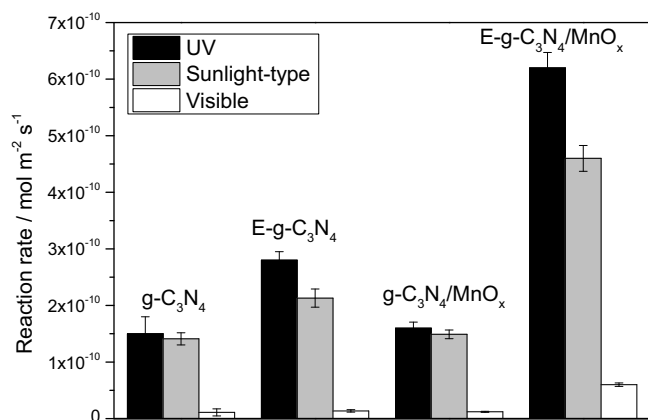**Fig. 8.** Surface area normalized reaction rate for the carbon nitride based samples.

Fig. 10. Quantum efficiency for the carbon nitride based samples.

To compare the sample performance on quantitative basis the calculation of the true quantum efficiency must be carried out. This is here computed following the recipes presented in Section 2.4.2, which require the local superficial rate of photon absorption, $e^{a,s}$, calculation as well as the measurement of the selectivity of the reaction. The obtention of the $e^{a,s}$ observable requires, according to Figs. 1 and 2, calculation on a cylindrical geometry and thus two independent geometrical variables. The local superficial rate of photon absorption observable across the corresponding two dimension reaction coordinates are presented in Fig. 9 under all (UV, visible and sunlight-type) illumination conditions tested in the study. The panels of Fig. 9 indicate the same geometrical behavior for all samples under study and thus differences between samples $e^{a,s}$ can be represented by a single number, the average value of $e^{a,s}$. Using thus the average values of data presented in Fig. 9, the selectivity information of Table 2 and Eq. (12) we computed the true quantum efficiency values under all illumination conditions tested.

Fig. 10 provides a graphical representation of the true quantum efficiency values obtained in the toluene photo-degradation using our carbon nitride containing catalysts. The comparison of the effi-
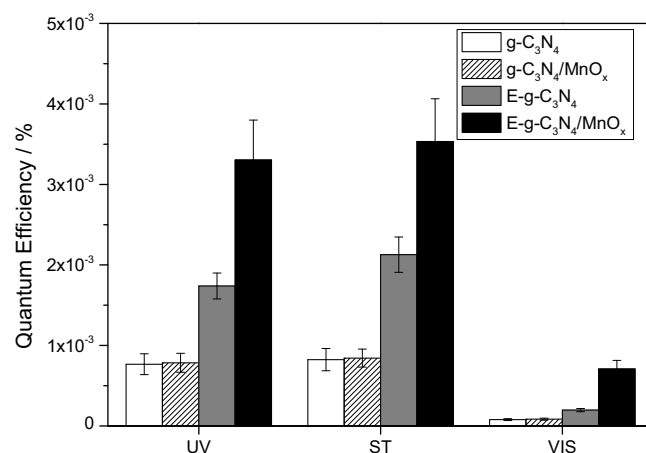
ciency values indicates the relatively high performance achieved under sunlight-type and UV excitation while significantly lower values are presented under visible light. Maximum values for all catalysts are obtained under sunlight-type excitation. This contrast (although differences are modest) with the reaction rate, displaying in the last case maximum values under UV.

The comparison of catalyst's performance is carried out in Table 3. In this table and by providing the ratio between the efficiency parameter of bulk and exfoliated samples as well as in presence or absence of MnO_x we attempt to measure in quantitative basis the influence of the exfoliation or the surface modification with Mn of the carbon nitride material. The surface deposition of MnO_x rendered, as mentioned, rather similar species in terms of their physico-chemical variables for both bulk and exfoliated samples but the catalytic effect as measured in Table 3 is different. The comparison of Mn-containing bulk and exfoliated carbon nitride materials vs. their bare counterparts (first two rows of Table 3) indicates an almost ×2 enhancement in the exfoliated case under UV and Sunlight-type illumination and of more than three times in the case of visible light. No significant differences are encoun-
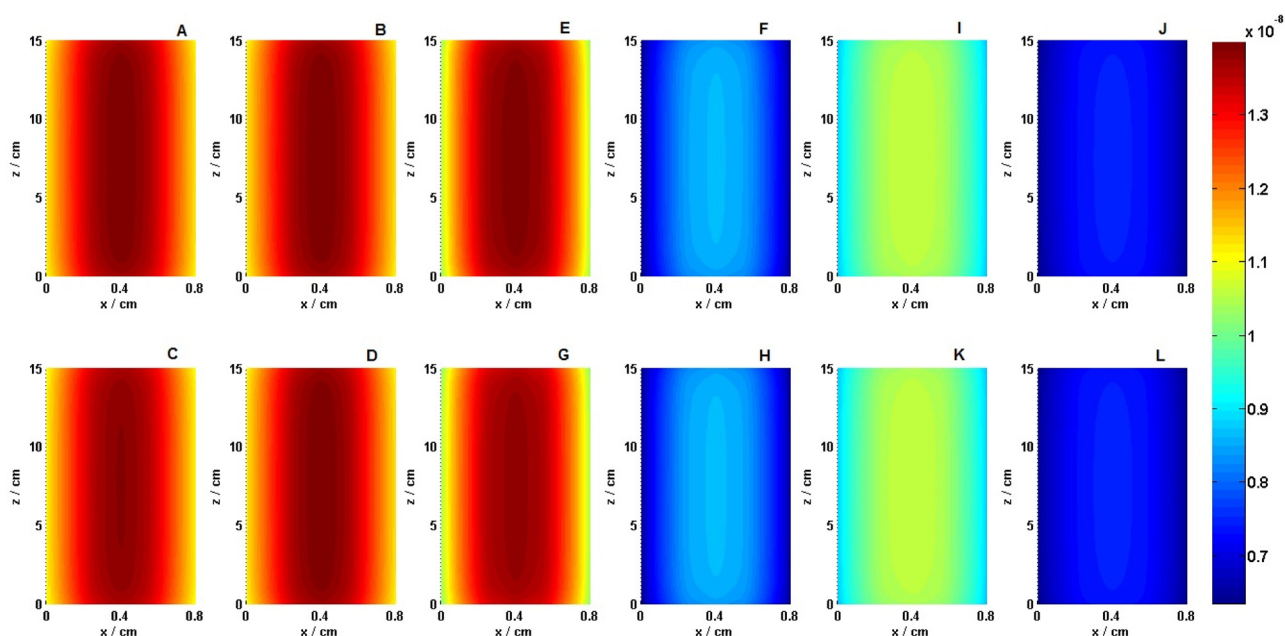

Fig. 9. Local superficial rate of photon absorption (Einstein cm^{-2} s^{-1}) of the samples under the different irradiation conditions (UV, sunlight-type and visible). The presentation of the panel follow this sequence: g-C$_3$N$_4$, E-g-C$_3$N$_4$, g-C$_3$N$_4$/MnO$_x$ and E-g-C$_3$N$_4$/MnO$_x$. From A to D (UV). From E to F (Sunlight-type). From I to L (Visible).

Table 3
Enhancement ratio produced by the presence of MnO_x species or the exfoliation process in toluene photodegradation quantum efficiency by carbon nitride samples.[a]

True Quantum Efficiency Ratio	UV	Sunlight-type	Visible
MnOx Effect			
g-C3N4/MnOx vs. g-C3N4	1.0	1.0	1.1
E-g-C3N4/MnOx vs. E-g-C3N4	1.9	1.7	3.6
Exfoliation Effect			
E-g-C3N4 vs. g-C3N4	2.3	2.6	2.5
E-g-C3N4/MnOx vs. g-C3N4/MnOx	4.2	4.2	8.4

[a] Average standard error: 31%.

Table 4
Excess function (defined by the ratio between the observable measured for sample E-g-C3N4/MnOx and Eq. (14)) produced by the simultaneous presence of surface MnO_x species and the exfoliation process of carbon nitride in toluene photodegradation quantum efficiency.[a]

Measurement	UV	Sunlight-type	Visible
E-g-C3N4/MnOx Quantum Efficiency	3.3×10^{-3}	3.5×10^{-3}	7.1×10^{-4}
Eq. (14)	1.7×10^{-3}	$1.9_5 \times 10^{-3}$	2.0×10^{-4}
Excess Function	1.9	1.8	3.5_5

[a] Average standard error: Quantum efficiency 20.5%; Excess Function 26%.

tered in the case of the bulk carbon nitride material. The differential catalytic effect of Mn in bulk-type and exfoliated carbon nitride materials has not obvious roots as Mn oxidation and dispersion state seem rather similar in both types of samples. A more efficient electronic interaction with the exfoliated support by effect of electronic confinement may be envisaged but requires further study to be substantiated.

The catalytic effect of the exfoliation process is measured and presented in the last two rows of Table 3. The enhancement ratio is always positive and larger than the effect ascribable to the presence of MnO_x species in the bulk or exfoliated carbon nitride materials. An increase of the efficiency related to the exfoliation process of ca of 2.5 times is observed for all illumination conditions in absence of Mn. In presence of Mn, we encountered ca. $\times 2$ enhancement with respect to the one presented in absence of such chemical species under UV and Sunlight-type illumination conditions and a further $\times 4$ in the case of Visible illumination. As a result of the carbon nitride dual modification, we observe an efficiency increase of ca. $\times 4$ (UV and Sunlight-type) or $\times 8$ (Visible) with respect to the bare carbon nitride sample. The exfoliation effect in photo-activity can be ascribed to the above described confinement effect in the electronic properties of the carbon nitride material.

From the previous numbers we can conclude that a consistent, positive (enhancement) effect induced by both the presence of surface MnO_x species and the exfoliation process. Quantitative measure (as presented in Table 3) of both modifications of the carbon nitride material indicates the similar (magnitude) catalytic effects produced under UV and Sunlight-type and a more important enhancement taking place under visible illumination. This quantitative estimation indicates that the energy of the charge carriers after light absorption influences strongly photo-activity, being the effect maximized under Sunlight (Fig. 10) by an effect mostly ascribable to UV photons, but the estimation also shows that the enhancement effect due to the presence of MnO_x presence or the exfoliation process have a more pronounced positive effect for visible rather than UV photons. However, visible photons do not generate chemistry to the level of UV photons. Table 3, on the other hand, does not provide a complete answer as to measure and understand the effect of these two modifications of the bulk carbon nitride material. Although the effect of MnO_x is barely observed in the case of the bulk materials and always of lower magnitude (roughly two times) than the one of the exfoliation process, the comparison of enhancement values of the two first as well as the two last columns of Table 3 indicates that, in addition to their "isolated", positive effects in the original bulk carbon nitride material, there is a synergistic effect between the two physical modifications of the bulk carbon nitride material.

To measure on quantitative basis the synergistic effect using the true efficiency parameter we present in Table 4 an excess (or synergy) function. A simple function of the henceforth called ideal, ternary system (where the effects of both physical modifications of the bulk carbon nitride materials are simultaneously present) can

be defined with respect to the main reference (bulk carbon nitride) and the parent binary (i.e. having a single modification) systems [33]:

$$\eta_q(E/MnO_x) = \eta_q(g-C_3N_4) + (\eta_q(E-g-C_3N_4) - \eta_q(g-C_3N_4))$$
$$+ (\eta_q(g-C_3N_4/MnO_x) - \eta_q(g-C_3N_4)) \tag{14}$$

Eq. (14) is defined to provide a way to measuring quantitatively if the physical modification triggered jointly by the exfoliation (right-hand side second term of the equation) or the presence of surface MnO_x species (right-hand side third term of the equation) in the bulk g-C3N4 catalyst is detrimental, positive but simply additive or, as expected in a good photocatalyst, synergistic. The ratio between the real, measured efficiency for the E-g-C3N4/MnOx sample and that corresponding to the mentioned ideal, ternary system η_q (E/MnOx; ideal) corresponds to an "excess" function which can be lower, equal or higher than 1. The set of the above mentioned observables concerning the E-g-C3N4/MnOx sample efficiency, the outcome of Eq. (14) and the excess ratio are presented in Table 4.

Inspection of the first two rows clearly indicates that combination of the two physical modifications of the bulk carbon nitride material generates a significant synergistic catalytic effect as measured through the true quantum efficiency. The third row quantifies the synergy in catalytic terms, indicating that the combined action of surface MnO_x species and the exfoliation has a roughly $\times 2$ (UV and Sunlight-type) or $\times 3.5$ (Visible) enhancement with respect to the isolated effect generated by each one. This therefore provides a quantitative measurement of the catalytic effects played by both modifications of the carbon nitride component indicating that the synergy between them is wavelength dependent but always significant (2–4 times).

4. Conclusions

In this work we synthesized a bulk-type, relatively low surface area carbon nitride material through a well-established procedure consisting on the calcination of a melamine precursor in a semi-closed system. The obtained semiconductor was subjected to physical modification related to a sono-assisted exfoliation process in water as well as to a surface deposition of Mn-containing species through an impregnation process. The physico-chemical properties of the resulting photocatalysts were measured and analyzed using a set of characterization techniques. The overall analysis of these studies indicates that the exfoliation treatment is effective in producing a less packed material having physico-chemical (particularly evidenced in the XRD, TEM and UV–vis data) properties affected by confinements affects derived from a delamination process. The study also showed that Mn species supported in the carbon nitride materials do not display significant differences in terms of the oxidation state and dispersion between the exfoliated and bulk carbon nitride samples.

Through the measurement of the optical properties of the system (materials and reactor constituents) and mathematical modeling we computed the true quantum efficiency for the photo-

degradation of toluene. Values of the true quantum efficiency allow to quantitatively estimating the catalytic effect of the two physical modifications suffered by the initial, bulk-type carbon nitride semiconductor. Although the two modifications are positive (or non-negative), we observe that the exfoliation process promotes activity about two times more efficiency that the surface Mn-containing species irrespective of the photon wavelength, i.e. for all UV and visible light photons, or the surface area of the carbon nitride material. Moreover, a strong synergistic effect, again two times with respect to the sum of the "isolated" components, is also observed when carbon nitride is subjected simultaneously to both modifications. The procedure here outlined for the analysis of the true quantum efficiency parameter provides a simple route to quantitative estimate and interpret the catalytic effects originated by physical modifications of carbon nitride materials and can be generalized to all photocatalytic materials and tests for composite, ternary materials.

Acknowledgement

Appendix A. Supplementary data

Supplementary data associated with this article can be found, in the online version, at http://dx.doi.org/10.1016/j.apcatb.2016.10.044.

References

[1] A. Kubacka, M. Fernández-García, G. Colón, Advanced nanoarchitectures for solar photocatalytic applications, Chem. Rev. 112 (2012) 1555–1614, http://dx.doi.org/10.1021/cr100454n.

[2] M.R. Hoffmann, S.T. Martin, W. Choi, D.W. Bahnemann, Environmental applications of semiconductor photocatalysis, Chem. Rev. 95 (1995) 69–96, http://dx.doi.org/10.1021/cr00033a004.

[3] Z. Wang, Y. Liu, B. Huang, Y. Dai, Z. Lou, G. Wang, X. Zhang, X. Qin, Progress on extending the light absorption spectra of photocatalysts, Phys. Chem. Chem. Phys. 16 (2014) 2758–2774, http://dx.doi.org/10.1039/c3cp53817f.

[4] L. Jing, W. Zhou, G. Tian, H. Fu, Surface tuning for oxide-based nanomaterials as efficient photocatalysts, Chem. Soc. Rev. 42 (2013) 9509–9549, http://dx.doi.org/10.1039/c3cs60176e.

[5] X. Chen, S.S. Mao, Titanium dioxide nanomaterials: synthesis, properties, modifications, and applications, Chem. Rev. 107 (2007) 2891–2959, http://dx.doi.org/10.1021/cr0500535.

[6] M.J. Muñoz-Batista, A. Kubacka, R. Rachwalik, B. Bachiller-Baeza, M. Fernández-García, Green photo-oxidation of styrene over W-Ti composite catalysts, J. Catal. 309 (2014) 428–438, http://dx.doi.org/10.1016/j.jcat.2013.10.021.

[7] M.M. Ballari, J. Carballada, R.I. Minen, F. Salvadores, H.J.H. Brouwers, O.M. Alfano, A.E. Cassano, Visible light TiO2 photocatalysts assessment for air decontamination, Process Saf. Environ. Prot. (2015), http://dx.doi.org/10.1016/j.psep.2015.08.003.

[8] S.M. Zacarías, M.L. Satuf, M.C. Vaccari, O.M. Alfano, Photocatalytic inactivation of bacterial spores using TiO2 films with silver deposits, 266 (2015) 133-140. 10.1016/j.cej.2014.12.074.

[9] A.L. Linsebigler, G. Lu, J.T. Yates, Photocatalysis on TiO2 surfaces: principles, mechanisms, and selected results, Chem. Rev. 95 (1995) 735–758, http://dx.doi.org/10.1021/cr00035a013.

[10] M.N. Gómez-Cerezo, M.J. Muñoz-Batista, D. Tudela, M. Fernández-García, A. Kubacka, Composite Bi2O3-TiO2 catalysts for toluene photo-degradation: ultraviolet and visible light performances, Appl. Catal. B Environ. 156–157 (2014) 307–313, http://dx.doi.org/10.1016/j.apcatb.2014.03.024.

[11] M.J. Muñoz-Batista, M.N.M.N. Gómez-Cerezo, A. Kubacka, D. Tudela, M. Fernández-García, Role of interface contact in CeO2-TiO2 photocatalytic composite materials, ACS Catal. 4 (2014) 63–72, http://dx.doi.org/10.1021/cs400878b.

[12] U. Caudillo-Flores, M.J.M.J. Muñoz-Batista, F. Ung-Medina, G. Alonso-Núñez, A. Kubacka, J.A.J.A. Cortés, M. Fernández-García, Effect of the anatase-rutile contact in gas phase toluene photodegradation quantum efficiency, Chem. Eng. J. 299 (2016) 393–402, http://dx.doi.org/10.1016/j.cej.2016.04.090.

[13] U. Caudillo-Flores, J. Lara-Romero, J. Zárate-Medina, M.J. Muñoz-Batista, R. Huirache-Acuña, E.M. Rivera-Muñoz, J.A. Cortés, Enhanced photocatalytic activity of MWCNT/TiO2 heterojunction photocatalysts obtained by microwave assisted synthesis, Catal. Today 266 (2016) 102–109, http://dx.doi.org/10.1016/j.cattod.2015.12.005.

[14] Z. Zhao, Y. Sun, F. Dong, Graphitic carbon nitride based nanocomposites: a review, Nanoscale 7 (2015) 15–37, http://dx.doi.org/10.1039/c4nr03008g.

[15] G. Dong, Y. Zhang, Q. Pan, J. Qiu, A fantastic graphitic carbon nitride (g-C3N4) material: electronic structure, photocatalytic and photoelectronic properties, J. Photochem. Photobiol. C Photochem. Rev. 20 (2014) 33–50, http://dx.doi.org/10.1016/j.jphotochemrev.2014.04.002.

[16] W.-J. Ong, L.-L. Tan, Y.H. Ng, S.-T. Yong, S.-P. Chai, Graphitic carbon nitride (g-C3N4)-based photocatalysts for artificial photosynthesis and environmental remediation: are we a step closer to achieving sustainability? Chem. Rev. (2016), http://dx.doi.org/10.1021/acs.chemrev.6b00075, acs.chemrev.6b00075.

[17] G. Mamba, A.K. Mishra, Graphitic carbon nitride (g-C3N4) nanocomposites: a new and exciting generation of visible light driven photocatalysts for environmental pollution remediation, Appl. Catal. B Environ. 198 (2016) 347–377, http://dx.doi.org/10.1016/j.apcatb.2016.05.052.

[18] S. Cao, J. Low, J. Yu, M. Jaroniec, Polymeric photocatalysts based on graphitic carbon nitride, Adv. Mater. 27 (2015) 2150–2176, http://dx.doi.org/10.1002/adma.201500033.

[19] Y. Cui, Y. Wang, H. Wang, F. Chen, Graphitic carbon nitrides: modifications and applications in environmental purification, Prog. Chem. 28 (2016) 428–437, http://dx.doi.org/10.7536/PC151025.

[20] M.J. Muñoz-Batista, O. Fontelles-Carceller, M. Ferrer, M. Fernández-García, A. Kubacka, Disinfection capability of Ag/g-C3N4 composite photocatalysts under UV and visible light illumination, Appl. Catal. B Environ. 183 (2016) 86–95, http://dx.doi.org/10.1016/j.apcatb.2015.10.024.

[21] J. Xue, S. Ma, Y. Zhou, Z. Zhang, M. He, Facile photochemical synthesis of Au/Pt/g-C3N4 with plasmon-Enhanced photocatalytic activity for antibiotic degradation, ACS Appl. Mater. Interfaces 7 (2015) 9630–9637, http://dx.doi.org/10.1021/acsami.5b01212.

[22] W.-J. Ong, L.-L. Tan, S.-P. Chai, S.-T. Yong, Heterojunction engineering of graphitic carbon nitride (g-C 3 N4) via Pt loading with improved daylight-induced photocatalytic reduction of carbon dioxide to methane, Dalt. Trans. 44 (2015) 1249–1257, http://dx.doi.org/10.1039/C4DT02940B.

[23] M. Faisal, A.A. Ismail, F.A. Harraz, S.A. Al-Sayari, A.M. El-Toni, M.S. Al-Assiri, Synthesis of highly dispersed silver doped g-C3N4 nanocomposites with enhanced visible-light photocatalytic activity, Mater. Des. 98 (2016) 223–230, http://dx.doi.org/10.1016/j.matdes.2016.03.019.

[24] L.-L. Ding, J.-P. Ge, W.-Q. Zhou, J.-P. Gao, Z.-Y. Zhang, Y. Xiong, Nanogold-functionalized g-C3N4 nanohybrids for sensitive impedimetric immunoassay of prostate-specific antigen using enzymatic biocatalytic precipitation, Biosens. Bioelectron. 85 (2016) 212–219, http://dx.doi.org/10.1016/j.bios.2016.04.102.

[25] J. Qin, J. Huo, P. Zhang, J. Zeng, T. Wang, H. Zeng, Improving the photocatalytic hydrogen production of Ag/g-C 3 N 4 nanocomposites by dye-sensitization under visible light irradiation, Nanoscale 8 (2016) 2249–2259, http://dx.doi.org/10.1039/C5NR06346A.

[26] N. Cheng, J. Tian, Q. Liu, C. Ge, A.H. Qusti, A.M. Asiri, A.O. Al-Youbi, X. Sun, Au-nanoparticle-loaded graphitic carbon nitride nanosheets: Green photocatalytic synthesis and application toward the degradation of organic pollutants, 5 (2013) 6815-6819. 10.1021/am401802r.

[27] S. Martha, A. Nashim, K.M. Parida, Facile synthesis of highly active g-C3N4 for efficient hydrogen production under visible light, J. Mater. Chem. A. 1 (2013) 7816, http://dx.doi.org/10.1039/c3ta10851a.

[28] Y. Di, X. Wang, A. Thomas, M. Antonietti, Making metal-carbon nitride heterojunctions for improved photocatalytic hydrogen evolution with visible light, ChemCatChem 2 (2010) 834–838, http://dx.doi.org/10.1002/cctc.201000057.

[29] Y. Bu, Z. Chen, W. Li, Using electrochemical methods to study the promotion mechanism of the photoelectric conversion performance of Ag-modified mesoporous g-C3N4 heterojunction material, 144 (2014) 622-630. 10.1016/j.apcatb.2013.07.066.

[30] L. Ge, C. Han, J. Liu, Y. Li, Enhanced visible light photocatalytic activity of novel polymeric g-C3N4 loaded with Ag nanoparticles, Appl. Catal. A Gen. 409–410 (2011) 215–222, http://dx.doi.org/10.1016/j.apcata.2011.10.006.

[31] M.J. Muñoz-Batista, A. Kubacka, A.B. Hungría, M. Fernández-García, Heterogeneous photocatalysis: light-matter interaction and chemical effects in quantum efficiency calculations, J. Catal. 330 (2015) 154–166, http://dx.doi.org/10.1016/j.jcat.2015.06.021.

[32] C. Miranda, H. Mansilla, J. Yáñez, S. Obregón, G. Colón, Improved photocatalytic activity of g-C3N4/TiO2 composites prepared by a simple impregnation method, J. Photochem. Photobiol. A Chem. 253 (2013) 16–21, http://dx.doi.org/10.1016/j.jphotochem.2012.12.014.

[33] M.J. Muñoz-Batista, A. Kubacka, M. Fernández-García, Effective enhancement of TiO2 photocatalysis by sinergistic interaction of surface species: from promoters to Co-Catalysts, ACS Catal. 4 (2014) 4277–4288, http://dx.doi.org/10.1021/cs501408u.

[34] T. Ohno, N. Murakami, T. Koyanagi, Y. Yang, Photocatalytic reduction of CO2 over a hybrid photocatalyst composed of WO3 and graphitic carbon nitride (g-C3N4) under visible light, J. CO2 Util. 6 (2014) 17–25, http://dx.doi.org/10.1016/j.jcou.2014.02.002.

[35] J. Chen, S. Shen, P. Guo, M. Wang, P. Wu, X. Wang, L. Guo, In-situ reduction synthesis of nano-sized Cu2O particles modifying g-C3N4 for enhanced photocatalytic hydrogen production, Appl. Catal. B Environ. 152 (2014) 335–341, http://dx.doi.org/10.1016/j.apcatb.2014.01.047.

[36] Z. Li, Y. Wu, G. Lu, Highly efficient hydrogen evolution over Co(OH)2 nanoparticles modified g-C3N4 co-sensitized by Eosin Y and Rose Bengal under visible light irradiation, Appl. Catal. B Environ. 188 (2016) 56–64, http://dx.doi.org/10.1016/j.apcatb.2016.01.057.

[37] J. Ma, C. Wang, H. He, Enhanced photocatalytic oxidation of NO over g-C3N4-TiO2 under UV and visible light, Appl. Catal. B Environ. 184 (2016) 28–34, http://dx.doi.org/10.1016/j.apcatb.2015.11.013.

[38] Y. Li, B. Wen, C. Yu, C. Chen, H. Ji, W. Ma, J. Zhao, Pathway of oxygen incorporation from O2 in TiO2 photocatalytic hydroxylation of aromatics: oxygen isotope labeling studies, Chemistry 18 (2012) 2030–2039, http://dx.doi.org/10.1002/chem.201103446.

[39] S. Obregón, G. Colón, Improved H2 production of Pt-TiO2/g-C3N4-MnOx composites by an efficient handling of photogenerated charge pairs, Appl. Catal. B Environ. 144 (2014) 775–782, http://dx.doi.org/10.1016/j.apcatb.2013.07.034.

[40] S. Obregón, Y. Zhang, G. Colón, Cascade charge separation mechanism by ternary heterostructured BiPO4/TiO2/g-C3N4 photocatalyst, 184 (2016) 96-103. 10.1016/j.apcatb.2015.11.027.

[41] M.J. Muñoz-Batista, A. Kubacka, M. Fernández-García, Effect of g-C3N4 loading on TiO2-based photocatalysts: UV and visible degradation of toluene, Catal. Sci. Technol. 4 (2014) (2006), http://dx.doi.org/10.1039/c4cy00226a.

[42] W. Peng, X. Li, Synthesis of MoS2/g-C3N4 as a solar light-responsive photocatalyst for organic degradation, Catal. Commun. 49 (2014) 63–67, http://dx.doi.org/10.1016/j.catcom.2014.02.008.

[43] M.J. Muñoz-Batista, M. Fernández-García, A. Kubacka, Promotion of CeO2-TiO2 photoactivity by g-C3N4: Ultraviolet and visible light elimination of toluene, Appl. Catal. B Environ. 164 (2015) 261–270, http://dx.doi.org/10.1016/j.apcatb.2014.09.037.

[44] X. Zhang, X. Xie, H. Wang, J. Zhang, B. Pan, Y. Xie, Enhanced photoresponsive ultrathin graphitic-phase C3N4 nanosheets for bioimaging, J. Am. Chem. Soc. 135 (2013) 18–21, http://dx.doi.org/10.1021/ja308249k.

[45] P. Niu, L. Zhang, G. Liu, H.-M. Cheng, Graphene-like carbon nitride nanosheets for improved photocatalytic activities, Adv. Funct. Mater. 22 (2012) 4763–4770, http://dx.doi.org/10.1002/adfm.201200922.

[46] Z. Ni, F. Dong, H. Huang, Y. Zhang, New insights into how Pd nanoparticles influence the photocatalytic oxidation and reduction ability of g-C3N4 nanosheets, Catal. Sci. Technol. 6 (2016) 6448–6458, http://dx.doi.org/10.1039/C6CY00580B.

[47] S.C. Yan, Z.S. Li, Z.G. Zou, Photodegradation performance of g-C3N4 fabricated by directly heating melamine, Langmuir 25 (2009) 10397–10401, http://dx.doi.org/10.1021/la900923z.

[48] M.J. Muñoz-Batista, A. Kubacka, M.N. Gómez-Cerezo, D. Tudela, M. Fernández-García, Sunlight-driven toluene photo-elimination using CeO2-TiO2 composite systems: a kinetic study, Appl. Catal. B Environ. 140–141 (2013) 626–635, http://dx.doi.org/10.1016/j.apcatb.2013.04.071.

[49] M.J. Muñoz-Batista, M. Ferrer, M. Fernández-García, A. Kubacka, Abatement of organics and Escherichia coli using CeO2-TiO2 composite oxides: ultraviolet and visible light performances, Appl. Catal. B Environ. 154–155 (2014) 350–359, http://dx.doi.org/10.1016/j.apcatb.2014.02.038.

[50] M.J. Muñoz-Batista, M.M. Ballari, A.E. Cassano, O.M. Alfano, A. Kubacka, M. Fernández-García, Ceria promotion of acetaldehyde photo-oxidation in a TiO2-based catalyst: a spectroscopic and kinetic study, Catal. Sci. Technol. 5 (2015) 1521–1531, http://dx.doi.org/10.1039/c4cy01293c.

[51] G.E. Imoberdorf, H.A. Irazoqui, A.E. Cassano, O.M. Alfano, Photocatalytic degradation of tetrachloroethylene in gas phase on TiO 2 films: a kinetic study, Ind. Eng. Chem. Res. 44 (2005) 6075–6085, http://dx.doi.org/10.1021/ie049185z.

[52] L. Palmisano, V. Augugliaro, R. Campostrini, M. Schiavello, A proposal for the quantitative assessment of heterogeneous photocatalytic processes, J. Catal. 143 (1993) 149–154, http://dx.doi.org/10.1006/jcat.1993.1261.

[53] O.M. Alfano, D. Bahnemann, A.E. Cassano, R. Dillert, R. Goslich, Photocatalysis in water environments using artificial and solar light, Catal. Today 58 (2000) 199–230, http://dx.doi.org/10.1016/S0920-5861(00)00252-2.

[54] R.J. Brandi, M.A. Citroni, O.M. Alfano, A.E. Cassano, Absolute quantum yields in photocatalytic slurry reactors, Chem. Eng. Sci. 58 (2003) 979–985, http://dx.doi.org/10.1016/S0009-2509(02)00638-3.

[55] A. Salinaro, A.V. Emeline, J. Zhao, H. Hidaka, V.K. Ryabchuk, N. Serpone, Terminology, relative photonic efficiencies and quantum yields in heterogeneous photocatalysis. Part II: experimental determination of quantum yields, Pure Appl. Chem. 71 (1999) 321–335, http://dx.doi.org/10.1351/pac199971020321.

[56] G. Li Puma, A. Brucato, Dimensionless analysis of slurry photocatalytic reactors using two-flux and six-flux radiation absorption-scattering models, Catal. Today. 122 (2007) 78–90, http://dx.doi.org/10.1016/j.cattod.2007.01.027.

[57] M.J. Muñoz-Batista, A. Kubacka, O. Fontelles-Carceller, D. Tudela, M. Fernández-García, M. Fernández-García, Surface CuO, Bi2O3, and CeO2 species supported in tiO2-anatase: study of interface effects in toluene photodegradation quantum efficiency, ACS Appl. Mater. Interfaces (2016), http://dx.doi.org/10.1021/acsami.6b03081, acsami.6b03081.

[58] J. Xu, L. Zhang, R. Shi, Y. Zhu, Chemical exfoliation of graphitic carbon nitride for efficient heterogeneous photocatalysis, J. Mater. Chem. A 1 (2013) 14766, http://dx.doi.org/10.1039/c3ta13188b.

[59] M.J. Muñoz-Batista, M.A. Nasalevich, T.J. Savenije, F. Kapteijn, J. Gascon, A. Kubacka, M. Fernández-García, Enhancing promoting effects in g-C3N4-Mn+/CeO2-TiO2 ternary composites: photo-handling of charge carriers, Appl. Catal. B Environ. 176–177 (2015) 687–698, http://dx.doi.org/10.1016/j.apcatb.2015.04.051.

[60] F. Dong, L. Wu, Y. Sun, M. Fu, Z. Wu, S.C. Lee, Efficient synthesis of polymeric g-C3N4 layered materials as novel efficient visible light driven photocatalysts, J. Mater. Chem. 21 (2011) 15171, http://dx.doi.org/10.1039/c1jm12844b.

[61] B. Chai, T. Peng, J. Mao, K. Li, L. Zan, Graphitic carbon nitride (g-C3N4)-Pt-TiO2 nanocomposite as an efficient photocatalyst for hydrogen production under visible light irradiation, Phys. Chem. Chem. Phys. 14 (2012) 16745, http://dx.doi.org/10.1039/c2cp42484c.

[62] Y. Wang, R. Shi, J. Lin, Y. Zhu, Enhancement of photocurrent and photocatalytic activity of ZnO hybridized with graphite-like C3N4, Energy Environ. Sci. 4 (2011) 2922, http://dx.doi.org/10.1039/c0ee00825g.

[63] H. Zhao, H. Yu, X. Quan, S. Chen, Y. Zhang, H. Zhao, H. Wang, Fabrication of atomic single layer graphitic-C3N4 and its high performance of photocatalytic disinfection under visible light irradiation, Appl. Catal. B Environ. 152 (2014) 46–50, http://dx.doi.org/10.1016/j.apcatb.2014.01.023.

[64] H. Yu, L. Shang, T. Bian, R. Shi, G.I.N. Waterhouse, Y. Zhao, C. Zhou, L.-Z. Wu, C.-H. Tung, T. Zhang, Nitrogen-doped porous carbon nanosheets templated from g-C 3 N 4 as metal-Free electrocatalysts for efficient oxygen reduction reaction, Adv. Mater. (2016) 1–7, http://dx.doi.org/10.1002/adma.201600398.

[65] L. Ma, H. Fan, J. Wang, Y. Zhao, H. Tian, G. Dong, Water-assisted ions in situ intercalation for porous polymeric graphitic carbon nitride nanosheets with superior photocatalytic hydrogen evolution performance, Appl. Catal. B Environ. 190 (2016) 93–102, http://dx.doi.org/10.1016/j.apcatb.2016.03.002.

[66] J. Yu, S. Wang, J. Low, W. Xiao, Enhanced photocatalytic performance of direct Z-scheme g-C3N4-TiO2 photocatalysts for the decomposition of formaldehyde in air, Phys. Chem. Chem. Phys. 15 (2013) 16883–16890, http://dx.doi.org/10.1039/c3cp53131g.

[67] C.D. Wagner, Handbook of x-ray photoelectron spectroscopy: a reference book of standard data for use in x-ray photoelectron spectroscopy, Physical Electronics Division, Perkin-Elmer Corp., 1979.

[68] H. Zhu, D. Chen, D. Yue, Z. Wang, H. Ding, In-situ synthesis of g-C3NTiO2 composite with enhanced visible light photoactivity, J. Nanoparticle Res. 16 (2632) (2014) 4–25, http://dx.doi.org/10.1007/s11051-014-2632-7.

[69] G. Marcì, M. Addamo, V. Augugliaro, S. Coluccia, E. Garcíía-López, V. Loddo, G. Martra, L. Palmisano, M. Schiavello, Photocatalytic oxidation of toluene on irradiated TiO2: comparison of degradation performance in humidified air, in water and in water containing a zwitterionic surfactant, J. Photochem. Photobiol. A Chem. 160 (2003) 105–114, http://dx.doi.org/10.1016/S1010-6030(03)00228-4.

[70] X. Chen, J. Wei, R. Hou, Y. Liang, Z. Xie, Y. Zhu, X. Zhang, H. Wang, Growth of g-C3N4 on mesoporous TiO2 spheres with high photocatalytic activity under visible light irradiation, Appl. Catal. B Environ. 188 (2016) 342–350, http://dx.doi.org/10.1016/j.apcatb.2016.02.012.

[71] F. Dong, Z. Wang, Y. Li, W.-K. Ho, S.C. Lee, Immobilization of polymeric g-C3N4 on structured ceramic foam for efficient visible light photocatalytic air purification with real indoor illumination, Environ. Sci. Technol. 48 (2014) 10345–10353, http://dx.doi.org/10.1021/es502290f.

[72] O. Fontelles-Carceller, M.J. Munoz-Batista, M. Fernandez-Garcia, A. Kubacka, M.J. Muñoz-Batista, M. Fernández-García, A. Kubacka, Interface effects in sunlight-Driven Ag/g-C3N4 composite catalysts: study of the toluene photodegradation quantum efficiency, ACS Appl. Mater. Interfaces 8 (2016) 2617–2627, http://dx.doi.org/10.1021/acsami.5b10434.